Conical Intersections in Solution: A QM/MM Study Using Floating Occupation Semiempirical Configuration Interaction Wave Functions

A. Toniolo,[†] G. Granucci,[‡] and Todd J. Martínez*,[†]

Department of Chemistry and The Beckman Institute, University of Illinois, Urbana, Illinois 61801, and Dipartimento di Chimica e Chimica Industriale, Università di Pisa, v. Risorgimento, Pisa, Italy

Received: November 21, 2002; In Final Form: February 25, 2003

We describe a hybrid quantum mechanical/molecular mechanical (QM/MM) method implemented in the context of floating-occupation molecular orbital semiempirical configuration interaction wave functions. The QM/MM approximation is compared to a fully QM treatment, emphasizing its accuracy with respect to features important to photochemical mechanisms such as conical intersection geometries and topography. The methodology we describe allows the location and characterization of solution-phase conical intersections for the first time. This is demonstrated explicitly by application to several biologically relevant chromophores solvated in clusters of up to 150 water molecules. The effect of solvation on the photochemical energy landscapes of these molecules is investigated, and we note a tendency for conical intersections to become absolute excited state minima upon hydration.

I. Introduction

The modern understanding of photochemistry revolves around the presence of conical intersections, points (or more generally hypersurfaces) of true degeneracy between different electronic states.[1−3] Electronic structure theory studies have confirmed the existence of energetically accessible intersections in many photochemical reactions,[4,5] and gas-phase dynamical investigations are buttressing the idea that these intersections play a key role in photochemical mechanisms.[6−12] However, detailed studies of the role of conical intersections in condensed phases have been quite scarce, in large part because of the difficulty of obtaining accurate ground and excited state potential energy surfaces for large systems.

One possible avenue toward including condensed phase environments in photochemical simulations is the use of hybrid quantum mechanics/molecular mechanics (QM/MM) methods. In QM/MM methods as applied to solutions, one generally treats a solute molecule with some form of electronic structure theory and uses a cruder molecular mechanics force field description for the solvent. The choice of electronic structure theory method used is generally dictated by practical considerations of computational cost and can be either semiempirical or ab initio. The first QM/MM method was developed in the context of proteins by Warshel and Levitt,[13] with refinements by many subsequent workers.[14−25]

In most cases, applications of QM/MM methods have been restricted to reactions occurring exclusively on the ground electronic state. However, there have been attempts to also treat electronically excited states, primarily to determine solvatochromic shifts.[26−38] Reasonable results are obtained for these shifts, but the performance of these methods with respect to excited state potential energy *surfaces* has been largely unexplored. This is primarily because it is difficult to get a globally accurate description of the QM region with practically applicable electronic structure methods. In particular, within the context of semiempirical and conventional ab initio quantum chemistry methods, there is ample evidence that a multireference description is mandatory for excited state potential energy surfaces. This considerably increases the computational cost compared to ground state potential energy surfaces or vertical excitation energies of optically allowed states. It is not clear to what extent such considerations also apply to recently developed density functional theory (DFT) methods such as time-dependent DFT.[39] We use a semiempirical analogue of the state-averaged complete active space (CASSCF) method[40,41] for the QM region in this paper. Importantly, this allows us to describe conical intersection regions, where a balanced description of the electronic wave functions *must* have multireference character.

Olivucci and co-workers showed that steric effects of bulky functional groups, such as *t*-butyl, could be included in the calculation of excited-state potential energy surfaces with a simple QM/MM-like model.[42] They used this method to investigate conical intersection geometries and relaxation paths of *tert*-butyl substituted butadienes in the gas phase. This was the first (and until now the only) example of the characterization of conical intersections within a hybrid QM/MM model, but the complete neglect of an electrostatic QM/MM interaction limited it to isolated molecules.

In this paper, we locate and characterize, for the first time, conical intersections in models of condensed phase systems. Both static and dynamic tuning of conical intersections, and hence photochemical mechanisms, are expected in condensed phase photochemistry. In this work, we only consider static effects of the solvent on the geometries, energetics, and topographies of conical intersections. The influence of dynamic tuning is also very interesting, but we leave the study of these effects to future work. Nevertheless, it is worth noting that the essential machinery required to carry out "on-the-fly" QM/MM nonadiabatic multiple spawning[9,43] or surface-hopping[44,45] dynamics is presented here.

* To whom correspondence should be addressed.
[†] University of Illinois.
[‡] Università di Pisa.

10.1021/jp022468p CCC: $25.00
Published on Web 04/18/2003

II. Theory and Computational Method

As in the usual QM/MM methodology,[13−15] we partition the Hamiltonian of the system as follows:

$$\hat{H}_{TOT} = \hat{H}_{QM} + \hat{H}_{QM/MM} + \hat{H}_{MM} \quad (1)$$

Here $\hat{H}_{QM}$ is the usual molecular electrostatic Hamiltonian, $\hat{H}_{MM}$ describes the intersolvent and intrasolvent force field, whereas $\hat{H}_{QM/MM}$ couples the two subsystems. In the model we have adopted, the QM/MM interaction consists of two terms. First, there is an electrostatic interaction where the QM part of the molecule sees MM region as a collection of point charges centered on the MM atoms. The MM charges are the same ones which appear in the MM force field. Second, to introduce quantum dispersion and repulsion, van der Waals terms are also included. Thus, in atomic units

$$\hat{H}_{QM/MM} = -\sum_i \sum_m \frac{Z_m}{r_{im}} + \sum_\alpha \sum_m \frac{Z_\alpha Z_m}{R_{\alpha m}} + \sum_\alpha \sum_m 4\epsilon_\alpha m \left[\left(\frac{\sigma_{\alpha m}}{R_{\alpha m}} \right)^{12} - \left(\frac{\sigma_{\alpha m}}{R_{\alpha m}} \right)^{6} \right] \quad (2)$$

where i and α are QM indices for electrons and nuclei, respectively, m represents MM atoms, Z are nuclear (QM) or effective atomic (MM) charges, and ϵ and σ are the van der Waals parameters. As usual, the QM atoms must be classified according to the MM model chosen in order to define the $\epsilon_{\alpha m}$ and $\sigma_{\alpha m}$ parameters for the QM/MM interaction.

The self-consistent field (SCF) equations are solved including the QM/MM monoelectronic term in the Fock matrix (first term on the right-hand side in eq 2). Thus, the molecular orbitals are obtained in the field produced by the charge distribution of the solvent. The orbitals are determined using the floating occupation molecular orbital (FOMO) SCF procedure.[46] This technique allows partial occupation and therefore optimization of all of the orbitals included in an energy window around the Fermi level. The occupation numbers change with molecular geometry, ensuring orbital degeneracy when necessary, such as during bond breaking. In contrast to complete active space self-consistent field (CASSCF) methods,[41] the FOMO approach does not require a multiconfigurational wave function ansatz to populate virtual orbitals and constitutes a very effective and fast computational technique. As a consequence of the partial optimization of the more significant virtual orbitals, the accuracy of configuration interaction procedures including a limited subset of the virtual orbitals is significantly improved, much like in the improved virtual orbital and similar procedures.[47,48] The accuracy of the FOMO semiempirical approach in the context of photochemical applications has been investigated by us recently.[49] We found that conical intersection geometries were well-predicted in comparison to CASSCF ab initio calculations.

The CI energy of the electronic state K can be written as

$$E_K = \langle \psi_K | \hat{H}_{QM} + \hat{H}^{el,QM/MM} | \psi_K \rangle + E^{CVW,QM/MM} + E_{MM} = E_K^{QM} + \sum_{\mu\nu} P_{\mu\nu}^K H_{\mu\nu}^{el,QM/MM} + E^{CVW,QM/MM} + E_{MM} \quad (3)$$

where E_{MM} is the energy of the molecular mechanical subsystem, P^K is the density matrix which should be determined in the MM field, and $E^{CVW,QM/MM}$ is the point-charge and vdW part of the QM/MM interaction energy, which does not depend on the wave function in the QM region (the second and third terms on the right-hand side in eq 2). Note that the first of the two terms arising from the QM/MM interaction is state specific. As a consequence, each electronic state is subject to a different interaction with the surrounding environment, changing its energy accordingly.

Efficient algorithms for conical intersection searches and molecular dynamics using this method will require analytic derivatives of the QM/MM CI energy. It has already been shown how analytical derivatives for CI energies using FOMO−SCF orbitals can be computed,[46] and this has been further extended to QM/MM systems.[50] Here, we present the technique in more detail. The analytical derivative is obtained from the Hellmann−Feynmann theorem, as applied in the semiempirical context by Dewar and Liotard:[51]

$$\frac{\partial E_K}{\partial Q_x} = \mathbf{C}_K^\dagger \frac{\partial \mathbf{H}_{CI}}{\partial Q_x} \mathbf{C}_K + \mathbf{C}_K^\dagger \frac{\partial \mathbf{H}^{el,QM/MM}}{\partial Q_x} \mathbf{C}_K + \frac{\partial E^{CVW,QM/MM}}{\partial Q_x} + \frac{\partial E_{MM}}{\partial Q_x} \quad (4)$$

where Q_x indicates the coordinate of a generic atom, belonging to either of the QM or MM subsystems. The $\mathbf{C}_K$ vectors denote the CI eigenvectors and the $\mathbf{H}$ matrixes represent the corresponding Hamiltonian operator in the basis of the selected Slater determinants. The first term is the usual gradient of the CI energy already described elsewhere.[46] The second term takes into account the QM/MM interaction matrix elements, involving the one-electron integrals

$$K_{\mu\nu} = -\left\langle \chi_\mu \left| \sum_m \frac{Z_m}{|\vec{r} - \vec{R}_m|} \right| \chi_\nu \right\rangle \quad (5)$$

where m indexes MM atoms. In the spirit of the NDDO (neglect of diatomic differential overlap) approximation,[52,53] the K integrals are assumed to vanish unless both atomic basis functions reside on the same atom. Following the standard semiempirical treatment of integrals, K integrals where both basis functions reside on the same atom are evaluated using a multipole representation of the $\chi_\mu\chi_\nu$ charge distribution and neglecting charge penetration corrections.[54] These K integrals present no conceptual difficulties beyond the usual one-center, one-electron integrals. In practice, the first and second terms of eq 4 are computed simultaneously.

Now we can define the gradient difference vector

$$\vec{g}_{KL} = \frac{\partial}{\partial \vec{Q}} (\langle \psi_K | H_{TOT} | \psi_K \rangle - \langle \psi_L | H_{TOT} | \psi_L \rangle) \quad (6)$$

and the nonadiabatic coupling vector

$$\vec{h}_{KL} = \left\langle \psi_K \left| \frac{\partial}{\partial \vec{Q}} \right| \psi_L \right\rangle \quad (7)$$

In the case of the nonadiabatic coupling vector, the elements corresponding to MM coordinates are set to zero. This approximation is not strictly necessary but, as will be shown below, is quite a good approximation when the QM/MM decomposition is well-chosen. The nonadiabatic coupling vector is built in the manner already presented in our previous paper.[49]

Once these two vectors are defined, we are able to optimize minimal energy conical intersections (MECIs) using the algorithm introduced by Bearpark et al.[55] as modified and implemented previously in the semiempirical context.[49] Details will not be repeated here, but the procedure can be summarized by stating that the MECI is found by following the direction of a

vector which is a combination of the gradient of the upper electronic state, projected onto the branching plane defined by $\vec{g}_{KL}$ and $\vec{h}_{KL}$, and the gradient difference vector, weighted by the energy gap between the states.

In the following, we present the results of calculations performed with a development version of the MOPAC code[54] in which the FOMO procedure, the driver for the optimization of conical intersections, and the QM/MM Hamiltonian for CI wave functions were implemented. In the remainder of this paper, unless otherwise specified, the QM region uses the semiempirical FOMO−CI method with the AM1 Hamiltonian[56] and the MM region uses the OPLS−UA force field[57] with the SPC representation of water.[58]

III. Applications

We now apply the QM/MM methodology to a number of molecules which are interesting in the context of condensed-phase photochemistry. All of the chosen examples are biologically important chromophores which normally function in a protein environment. Ultimately, a QM/MM method of the type described here, augmented with a scheme for dealing with QM/MM boundaries across covalent bonds,[13,15−17,20,59] could be used to investigate photochemistry in the native protein environment, and work along these lines is currently in progress. However, in the present paper, we only compare features of the expected photochemistry in gas and solution phases.

It should be understood that, despite the greatly improved description of excited electronic states (compared to standard semiempirical methods) which comes from the FOMO−CASCI approach, the semiempirical method being used for the QM region has inherent limitations. We have previously characterized these for some of the very molecules investigated here.[49] In particular, the relative energetics of conical intersections predicted with standard parametrizations is often incorrect. At the same time, the FOMO−CASCI method with standard semiempirical parametrizations is often able to predict the qualitative geometries as well as the character of the electronic states involved in minimal energy conical intersections. Thus, the conclusions we make in this paper regarding the effect of solvation on conical intersections in these molecules are expected to be valid, but it would be pointless to do detailed dynamical simulations without reparametrization. Therefore, in this paper, we focus attention primarily on the changes in the ground and excited-state PESs in the neighborhood of the important conical intersections.

1. Static Solvent Effects on Intersection Energetics. Our first example is *p*-hydroxybenzylidene-imidazolidinone, the chromophore in green fluorescent protein (GFP). The GFP chromophore (autocatalytically formed by posttranslational modification from a Ser-Tyr-Gly sequence in the protein) exhibits significant fluorescence in the protein environment but is not fluorescent in liquid solution at room temperature.[60] It has been suggested[61] that the nonradiative decay observed in solution may be a consequence of conical intersections associated with torsion, and we have previously confirmed the existence of such intersections in the gas phase using both semiempirical FOMO−CI and ab initio methods.[49]

We have placed the GFP chromophore in a microsolvated environment, with 51 surrounding water molecules. The electronic structure treatment includes all excitations of 12 electrons in 8 active orbitals, FOMO−CASCI(12/8). An energy width of 0.2 hartree is used in the FOMO−SCF procedure. The geometry was constructed by placing water molecules in favorable hydrogen bonding arrangements around the polar groups of the chromophore, followed by energy minimization. This procedure is not expected to generate the global minimum but rather just a representative of the geometries that might be sampled in such a cluster. We follow the same procedure throughout this paper, noting that a detailed study of one chromophore would require accounting of the statistical nature of either a microsolvated cluster or bulk solution.

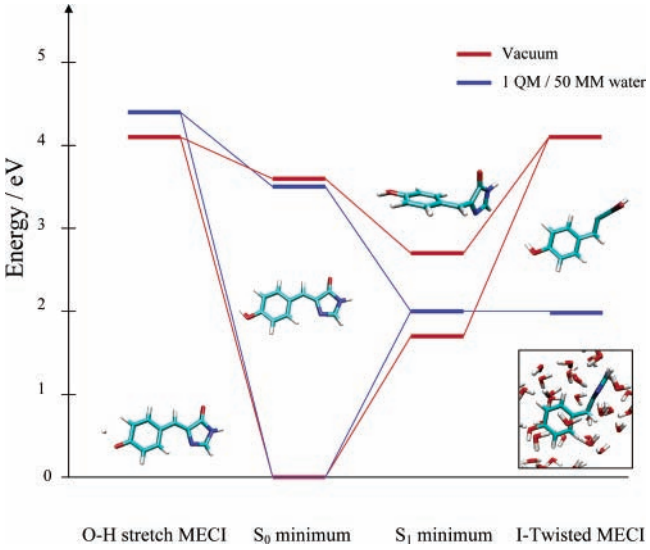

Figure 1. Energy level diagram of some important points on the S_0 and S_1 potential energy surfaces of the isolated (blue) and microsolvated (red) GFP chromophore. In both cases, the chromophore is treated with QM. One water molecule (H-bonded to the phenol ring) is treated as QM and the other 50 as MM in the microsolvated calculations. Geometries are reoptimized for each case. Notice that the lowest energy conical intersection ("I-Twisted MECI") becomes the minimum on S_1 in the microsolvated case, leading one to expect faster nonradiative decay in solution than in the gas phase.

TABLE 1: Comparison of the Relative Energies (in eV) of the Two Lowest Singlet States of the Isolated and Solvated GFP Chromophore at Its S_0 and S_1 Equilibrium Geometries and at Two S_0/S_1 Minimal Energy Conical Intersections[a]

	S_0 eq (a)	S_1 eq (b)		O−H stretch	I-twist
	S_1	S_0	S_1	MECI (c)	MECI (e)
vacuum	3.58	1.62	2.75	4.15	4.03
2 wat. (2 QM)	3.54	1.66	2.62	4.06	3.97
2 wat. (1 QM 1 MM)	3.79	1.80	2.60	4.42	4.25
2 wat (2MM)	3.81	1.82	2.56		4.27
51 wat. (1 QM 50 MM)	3.52	1.96	1.96	4.11	1.96

[a] The zero of energy is chosen as S_0 at the S_0 equilibrium geometry. Letters enclosed in parentheses refer to the corresponding geometries depicted in Figure 6 of ref 49. Three different QM/MM decompositions are compared for the case where the chromophore is surrounded by only two water molecules.

The GFP chromophore and one of the surrounding water molecules (closest to the OH group of the phenol ring) were treated with the QM method and the remaining 50 water molecules with the MM method. The QM treatment of one water molecule was motivated by suggestions that the phenolic proton is involved in proton transfer after photoexcitation.[60] We have computed excitation energies at the S_0 local minimum, searched for minima on S_1, and located minimal energy conical intersections (MECIs) corresponding to those we have previously characterized[49] in the isolated chromophore. The resulting energy landscape for the microsolvated cluster is compared with that for the isolated chromophore in Figure 1 (see also Table 1). In the gas phase, the chromophore has a well-defined local minimum on S_1 corresponding to twisting about the bond

connecting the bridging carbon atom and the imidazolinone ring (the "I-bond"). A minimal energy conical intersection ("I-twisted MECI") can be reached from the S_1 minimum by pyramidalization about one of the carbon atoms, but this is energetically unfavorable. With the standard AM1 parameters, the energy cost to reach this intersection is greater than 1 eV and, in fact, lies above the Franck−Condon point. There is a MECI involving extension of the phenolic O−H bond ("O−H stretch MECI"), but this is also energetically inaccessible from the Franck−Condon point. Ab initio calculations confirm this general picture, although the conical intersections lie considerably lower than found with FOMO−CI and AM1 parameters.[62]

Solvation induces a red-shift of the vertical excitation energy, but this is quite small. Similarly, the O−H stretch MECI is stabilized, but remains inaccessible from the Franck−Condon region. On the other hand, there is a dramatic effect on the I-twisted conical intersection, which is so strongly stabilized that it becomes the minimum on S_1. In other words, there is no true minimum on S_1 after solvation, but instead the absolute minimum is a conical intersection. After photoexcitation to S_1 in the gas phase, the molecule would be expected to move toward the region of the PES around the equilibrium geometry of S_1 before reaching the I-twisted MECI. In solution, the same I-twisted MECI becomes the S_1 minimum and can be expected to serve as a funnel for fast decay to the ground state. The prediction is therefore a marked decrease in the excited state lifetime going from the isolated chromophore to a solvated environment. Indeed, a significant ultrafast component to the decay of the GFP chromophore excited state has been observed in solution studies.[63]

One might inquire into the cause of solvent stabilization of the I-twisted MECI. Part of the answer may lie in the fact that the I-twisted MECI involves considerably less pyramidalization than in the gas phase. A more important observation concerns the particular behavior of the dipole moment of the two electronic states as a function of torsion about the I-bond. At the S_0 equilibrium geometry, the dipole moments of S_0 and S_1 are similar ($\approx$2 D). However, at the S_1 minimum, the dipole moments are quite different, with $\approx$1 D for S_0 and $\approx$10 D for S_1. Moreover, the direction of the dipole moment vector indicates a clear intramolecular electron transfer across the bridge from the phenol ring to the imidizalidinone ring. This is further supported by Mulliken analysis, which shows 0.8 electron charge units transferred from the phenol ring and bridge atoms to the imidizalidinone ring. Such charge separation is obviously stabilized in a polar solvent like water, with the consequence that the intersection arising from the interaction of neutral-like and charge-transfer-like electronic states is also strongly stabilized.

A second example is the chromophore of photoactive yellow protein (PYP). This protein is the primary receptor for negative phototaxis response in *Ectothiorodhospira haliphilia*. It is a small and soluble protein thought to be a useful model for biological signal transduction.[64] In the dark-adapted wild type protein, the chromophore is found as an anion which is protonated after photoexcitation. We study the neutral form of the PYP chromophore here, which has been experimentally studied in both gas[65] and condensed[66,67] phases. Again we optimized the ground state and the first singlet excited of the chromophore (where we have replaced the thioester by an ester linkage) at different conformations and also at some conical intersections. Figure 2 shows the conformations of the chromophore which we will discuss. The QM treatment in this case involved a CASCI with six electrons in six orbitals, i.e.,

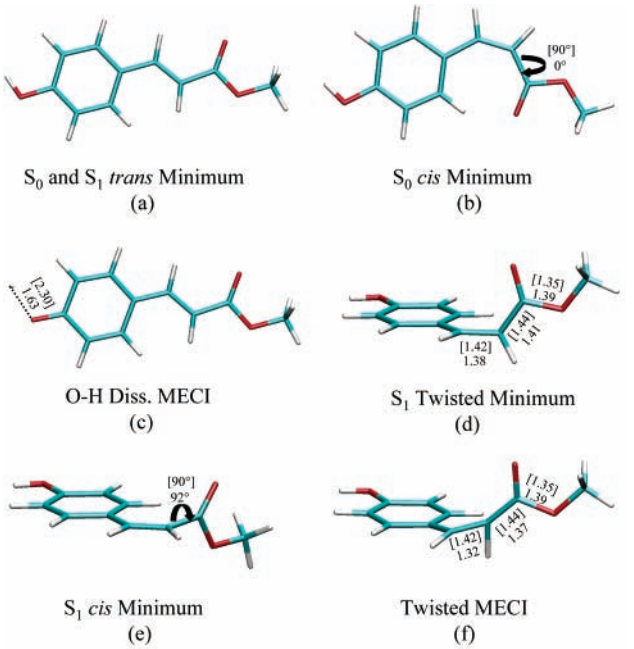

Figure 2. Photoactive yellow protein (PYP) chromophore equilibrium geometries for S_0 and S_1 and the lowest energy S_0/S_1 conical intersections. The S_1 trans minimum exists in the isolated molecule but not when solvated. Geometries e and f are distinct in the isolated molecule, but the same when solvated. Some geometrical parameters are given for the isolated and solvated (in square brackets) molecules. See text for details.

FOMO−CASCI(6/6) with an energy width of 0.2 hartree for the FOMO procedure. Again, one water molecule which is H-bonded to the phenol is included in the QM region and the MM region consists of 50 water molecules. The results of the optimizations are reported in Table 2. In both the ground and excited electronic states, the cis conformer is stabilized relative to the trans conformer, which is a consequence of the larger dipole moment in the cis conformer. Additionally, the S_1 minimum of the trans conformer disappears in the solution environment. The same behavior seen in the GFP chromophore is repeated here; the MECI involving torsion (Figure 2f) is dramatically stabilized and becomes the absolute minimum of the excited state. The reason is again that this intersection results from the interaction of charge-transfer-like and neutral-like electronic states. In the isolated chromophore, the dipole moment on S_0 and S_1 are the same (3.6 D) in the cis planar geometry, whereas these change to 11.7 D for S_1 and 3.9 D for S_0 upon twisting about the C−C double bond. Again, the intramolecular charge-transfer involves removing an electron from the phenolic ring.

It is interesting to note the similarities in the MECIs discussed for GFP and PYP chromophores and those previously discussed for ethylene. In the GFP chromophore, a carbon atom is pyramidalized at the I-twisted MECI, analogous to the behavior observed in the twisted/pyramidalized MECI of ethylene.[68] In the PYP chromophore, one of the hydrogen atoms in the central moiety nearly forms a bridge to a second carbon atom, much like that which is observed in the hydrogen migration intersection of ethylene.[68] As one might expect, the motifs seen in the conical intersections of small molecules tend to be repeated in related, larger molecules.

Our final example is an analogue of retinal protonated Schiff base (RPSB), which is the chromophore in the rhodopsin family of proteins. We follow the same procedure as before, with the chromophore defining the QM region and 57 water molecules

TABLE 2: Comparison of the Relative Energies (in eV) of the Two Lowest Singlet States of the Isolated and Solvated PYP Chromophore at Its S_0 and S_1 Equilibrium Geometries and at Two S_0/S_1 Minimal Energy Conical Intersections[a]

	S_0 trans eq (a)	S_0 cis eq (b)		S_1 trans eq (a)		S_1 cis eq (e)		S_1 twist eq (e)		twisted MECI (f)	O−H stretch MECI (c)
	S_1	S_0	S_1	S_0	S_1	S_0	S_1	S_0	S_1		
vacuum	3.77	0.23	4.01	0.15	3.63	0.28	3.69	1.88	3.06	3.96	4.55
51 wat. (1 QM 50 MM)	4.01	−0.18	3.62	not a minimum		0.03	3.43	2.05	2.05	2.05	4.90

[a] The zero of energy is chosen as S_0 at the S_0 trans equilibrium geometry. Letters enclosed in parentheses refer to the corresponding geometry depicted in Figure 6.

TABLE 3: As in Table 2, but for Retinal Protonated Schiff Base[a]

	S_0 eq (a)	S_1 eq 13−14 twist (b)		13−14 twisted MECI (e)	11−12 twisted MECI (c)	9−10 twisted MECI (f)	nitrogen pyram. MECI (d)
	S_1	S_0	S_1				
vacuum	2.22	0.90	1.79	2.24	1.31	1.63	2.11
57 wat. (57 MM)	2.87	1.12	1.12	1.12	1.63	1.92	2.15

[a] Letters enclosed in parentheses refer to the corresponding geometry depicted in Figure 8 of ref 49.

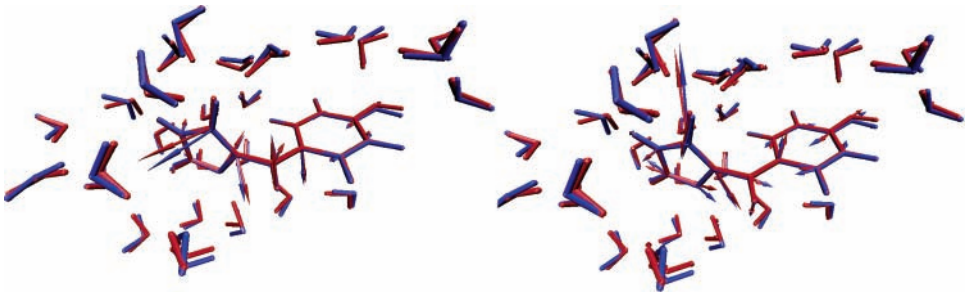

Figure 3. Comparison of optimized minimal energy conical intersection between S_0 and S_1 for the GFP chromophore surrounded by 27 water molecules using QM (blue) and QM/MM (red) methods. All but one of the water molecules are modeled with a MM force field in the QM/MM treatment. The nonadiabatic coupling ($\vec{h}$) and gradient difference ($\vec{g}$) vectors are compared in the left and right panels, respectively.

in the MM region. As a CASCI treatment of all π electrons led to an excessive number of configurations, we have limited the CI to at most triple excitations from a Hartree−Fock-like reference. All 10 π electrons are included in the CI, and eight orbitals have variable occupation in the CI; that is, the electronic wave function is CISDT(10/8). The FOMO procedure is again used, with an energy width of 0.15 hartree. The results for the chromophore in vacuum and surrounded by 57 water molecules are shown in Table 3. A pronounced blue shift of the vertical excitation energy is observed and expected because the charged nature of the chromophore will strongly orient the solvent to preferentially stabilize the ground state. Once again, the stabilization of a conical intersection such that it becomes an absolute minimum is observed; the $C_{13}-C_{14}$ twisted MECI, which is not even energetically accessible from the Franck−Condon point in vacuum, becomes the global S_1 minimum. The $C_{11}-C_{12}$ and C_9-C_{10} twisted MECIs are absolute minima already in the isolated molecule, and this is not changed upon solvation.

Previous ab initio results suggest that the $C_{11}-C_{12}$ and $C_{13}-C_{14}$ twisted MECIs are effectively degenerate for isolated RPSB,[69] which is in contrast to the vacuum FOMO semimepirical results in Table 3. This failure of the semiempirical method has been pointed out in our previous work,[49] and one might expect the detailed branching of photoproducts to be incorrectly predicted in solution without reparametrization. However, we do not comment further on this issue because dynamical simulations are required to determine the degree of (dis)agreement with experimentally determined photoproduct branching ratios.

2. Conical Intersection Topography with QM and QM/MM Methods. The topography of the potential energy surface around a conical intersection can have profound effects on the efficiency of quenching through the intersection. Atchity and Ruedenberg introduced a qualitative classification of the possible topographies, noting that the ensuing dynamics could be quite different in the various limiting cases.[70] Subsequently, Yarkony verified this effect for several model problems,[71] and we have shown that it provides a natural explanation for the observed photoproduct yields in retinal protonated Schiff base.[69] Because the intended application of the methodology developed here is in the context of nonadiabatic dynamics, e.g., photochemistry in solution and protein environments, it is therefore of keen interest to investigate the effect of the QM/MM approximation on intersection topography in addition to energetics. This includes both the nature of the molecular motions comprising the branching plane (formed by the $\vec{g}$ and $\vec{h}$ vectors) and also the form of the potential energy surfaces in this plane.

In the definition of the nonadiabatic coupling vector, we have assumed that the coordinates of the solvent, or more precisely, the MM atomic coordinates, do not affect the coupling between two electronic states of the solute. Although it is physically reasonable that the contribution of the solvent should in most cases be quite small, this is not guaranteed and must be validated directly. We have done this in the case of the GFP chromophore, computing the $\vec{g}$ and $\vec{h}$ vectors for the same solvated system with fully QM and QM/MM methods. Because the fully QM optimization of a conical intersection can be computationally challenging, we have reduced the number of solvating water molecules to 27. We have then optimized an "I-twisted" MECI, as described above, for the fully QM system. This geometry was used as an initial guess for a similar MECI search in the QM/MM method (where the chromophore and one water molecule were treated with QM and the remaining 26 water molecules were treated with an MM force field). The two resulting geometries are compared in Figure 3 and are in quite good overall agreement.

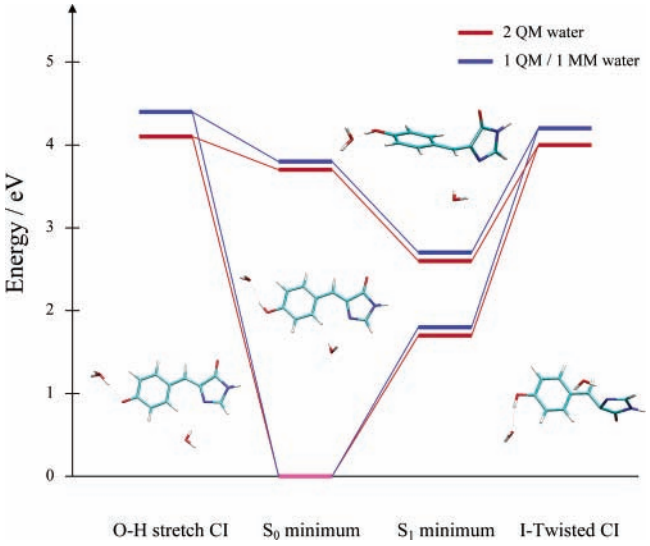

Figure 4. As in Figure 1, for the GFP chromophore solvated by two water molecules. Results of the QM and QM/MM methods are compared: red and blue indicate energies computed with QM or QM/MM, respectively. Geometries are reoptimized for QM and QM/MM methods.

We also compare the $\vec{g}$ and $\vec{h}$ vectors at the optimized MECI in the QM and QM/MM cases. Because of the degeneracy of the two electronic states at a conical intersection, it is really only the subspace spanned by these vectors as defined by eqs 12 and 13 that is relevant. There are several possible procedures for standardizing the vectors such that a clear comparison can be made.[2,49,72] We follow our previous work and choose the following procedure, which is guaranteed not to change the branching plane and allows for a clear comparison of the molecular motions involved in lifting the degeneracy around the intersection. We orthogonalize $\vec{h}$ to $\vec{g}$ using a Gram−Schmidt procedure. After obtaining an orthogonal pair of vectors in this way for the QM case, the QM/MM $\vec{g}$ and $\vec{h}$ are rotated between themselves to obtain maximal overlap between the QM and QM/MM $\vec{g}$. The sign of the QM/MM $\vec{h}$ is then chosen to agree with the QM $\vec{h}$. The resulting standardized $\vec{g}$ and $\vec{h}$ vectors are compared for the QM and QM/MM cases in the right and left panels of Figure 3, respectively. These are quite similar in the QM and QM/MM cases. A quantitative measure of the agreement is provided by the overlap between the corresponding QM and QM/MM vectors, which is computed to be 0.99 and 0.96 for the nonadiabatic coupling and energy difference gradient, respectively. The nonadiabatic coupling vector has no component in the MM region by construction, but one can see from the right panel of Figure 3 that the fully QM treatment also predicts negligible components here. Although this is encouraging, one should recognize that the particular QM/MM decomposition chosen will affect the validity of the approximation that the nonadiabatic coupling is nonzero only in the QM region. This assumption should therefore be tested on a case-by-case basis.

Given that the geometry of the MECI and the nature of the branching plane have not been unduly affected by the QM/MM approximation, it is now appropriate to ask about the topography of the intersection. First, we compare the QM/MM and fully QM results for the energetics relevant to photochemistry in a small system: the GFP chromophore surrounded by two water molecules. Figure 4 shows the energy landscape of the GFP chromophore with two water molecules using both QM and QM/MM approaches. In the QM/MM method, we treat one water molecule (the one which is not H-bonded to the phenol) using

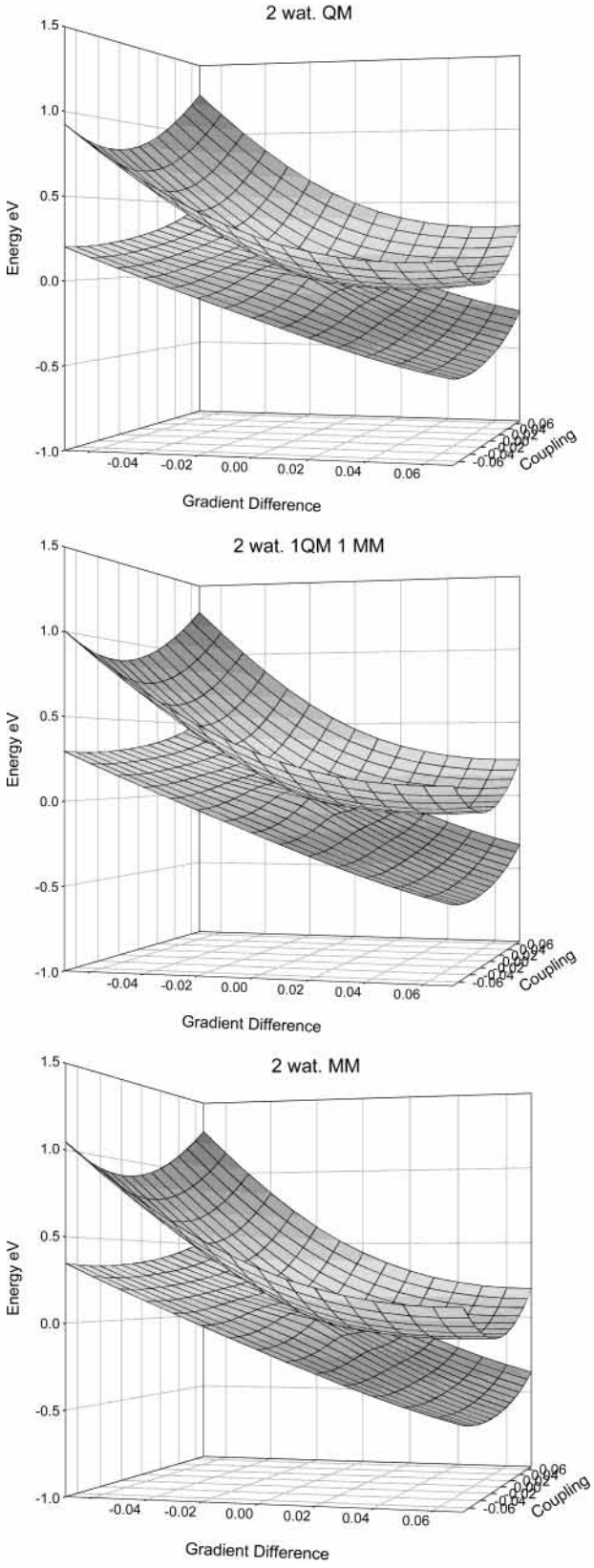

Figure 5. Comparison of the potential energy surface in the immediate neighborhood of a conical intersection using QM and QM/MM methods for the GFP chromophore in the presence of two water molecules. The potential energy surfaces are plotted in the "branching plane", given by the nonadiabatic coupling and gradient difference vectors. The chromophore is treated with the QM method in all three calculations. From top to bottom, the three panels depict calculations where both water molecules are QM, the water molecule H-bonded to the chromophore is QM, and both water molecules are treated with MM force fields.

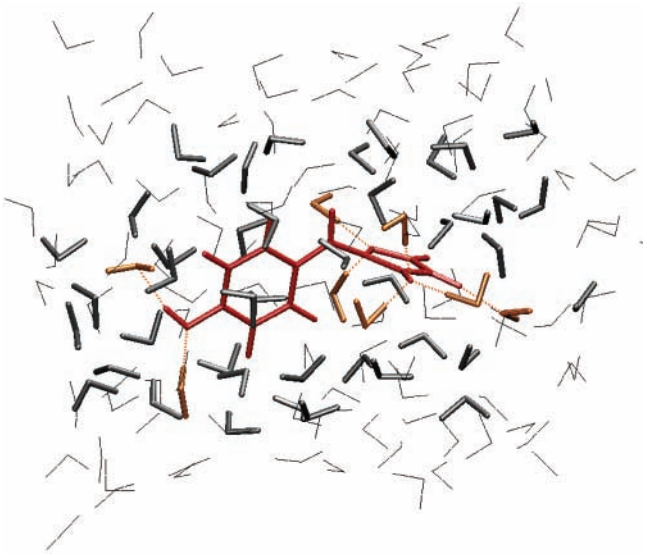

Figure 6. Depiction of a minimal energy "I-twisted" conical intersection of the GFP chromophore (red) solvated by one QM and 150 MM water molecules. Water molecules which are considered H-bonded to the chromophore are indicated in gold, and the first solvation shell is comprised of the gray and gold water molecules.

the MM method. One sees that the qualitative features of the potential energy landscape are quite similar, although there are of course differences in the details. The magnitude of these differences can be seen clearly in Table 1, where the vertical excitation energy, for example, is in error by less than 0.3 eV comparing the different QM and QM/MM treatments.

Now, we can compare the topography around the I-twisted intersection for all three QM/MM decompositions: zero, one, or two water molecules included with the chromophore in the QM region. We have optimized the intersection geometry and computed the branching plane vectors separately for each of these cases and then mapped the ground and excited state PES in the branching plane around the intersection. The results are shown in Figure 5, and one sees that the intersection is clearly sloped in all cases. Thus, at least for this case, the topography of the intersection is similar in the QM and QM/MM treatments.

The previous results seem to indicate that an MM representation of the solvent is a good approximation of the full QM solute−solvent interaction in the case of a couple of water molecules. It is also worthwhile to investigate a case with many water molecules. Thus, we have optimized the same MECI in the presence of one QM and 150 MM water molecules. In this case, we are no longer able to do the fully QM calculation. However, we can increase the size of the QM region. We do this in two stages, first including eight water molecules which are H-bonded to the solute, and finally including 51 water molecules which comprise the first solvation shell. The intersection geometry is shown in Figure 6, where the GFP chromophore appears in red, the H-bonded water molecules are gold, additional water molecules in the first solvation shell are gray, and the remaining water molecules which are always treated with MM force fields are light black lines. For the model where all but one of the water molecules are MM, we optimized the MECI geometry and computed the $\vec{g}$ and $\vec{h}$ vectors. Then, we computed cuts of the PES along the $\vec{g}$ and $\vec{h}$ vectors for each of the three QM/MM decompositions. The results are shown in Figure 7. As one might expect, the exact position of the conical intersection does depend on the QM/MM decomposition; only for the case where all water molecules are MM does one find

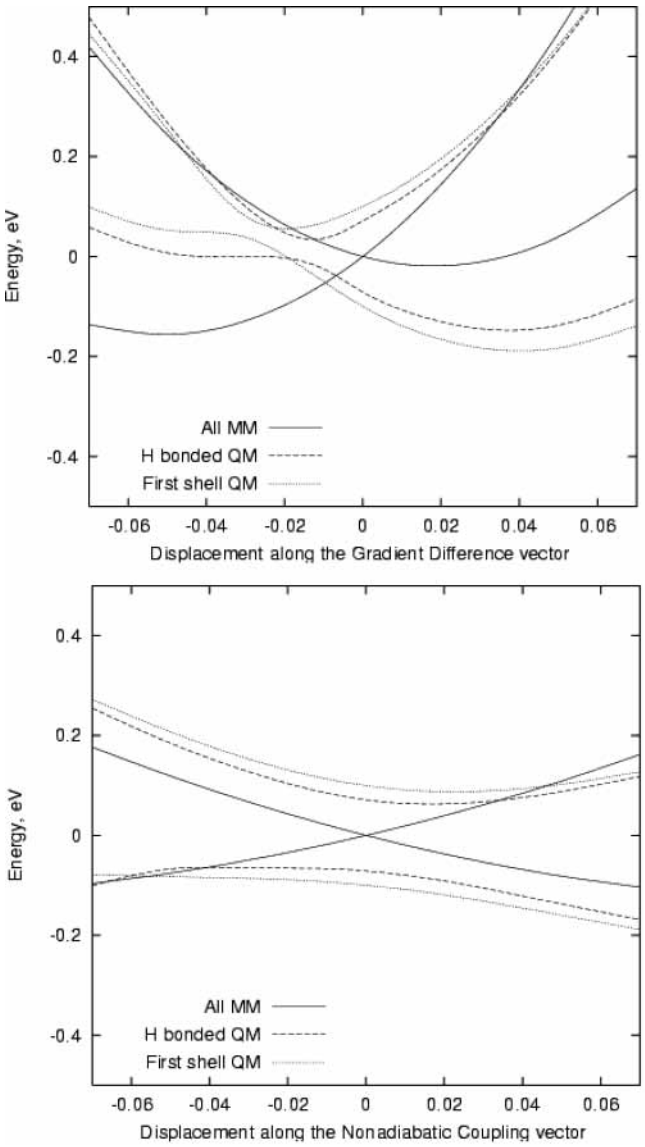

Figure 7. Comparison of the ground and excited state potential energy surfaces in the neighborhood of an "I-twisted" minimal energy conical intersection for the GFP chromophore surrounded by 150 water molecules. Cuts are along the gradient difference and nonadiabatic coupling vectors as indicated. The geometry and branching plane vectors are determined using a QM/MM method where all 150 water molecules are treated as MM. The calculations are repeated at the same geometries including H-bonded water molecules (8 water molecules, see Figure 6) or the entire first solvation shell (51 water molecules, see Figure 6) in the QM region. As should be expected, the conical intersection geometry clearly changes somewhat depending on the nature of the QM/MM decomposition. However, these changes are not very large in the present case.

exact degeneracy at zero displacement in both panels of Figure 7. However, the curves are all qualitatively quite similar, and the topography of the intersection is of the same sloped character in all three cases.

IV. Conclusions

We have described in detail a QM/MM approach built on a semiempirical methodology adapted to treat excited states: the floating-occupation molecular orbital configuration interaction (FOMO−CI) method. In previous work,[49] we have investigated the applicability of the FOMO−CI method to the problem of determining conical intersection geometries, topographies, and energetics in isolated molecules. Here, we have extended this

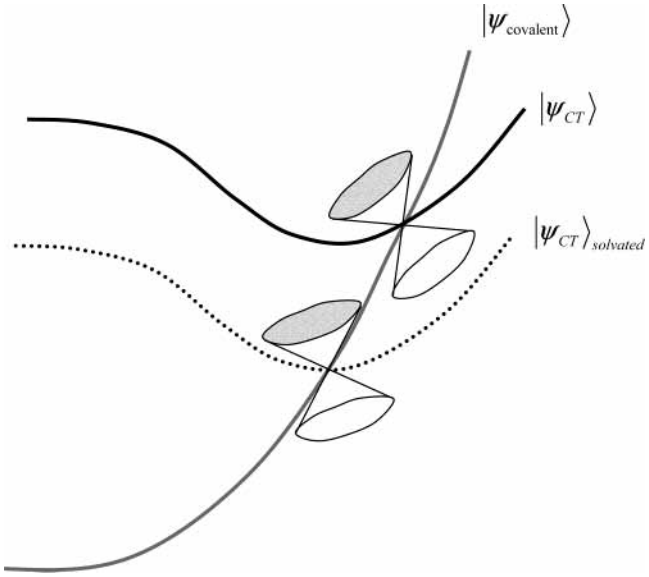

Figure 8. Schematic diagram illustrating how sloped intersections may become peaked upon polar solvation. The depicted intersection arises from the interaction of a charge transfer state, ψ_{CT}, and a covalent state, $\psi_{covalent}$. The covalent state is denoted by the solid gray line and is barely affected by solvation. The charge transfer state, shown as a solid black line in the isolated molecule, is strongly stabilized by solvation, shown as the dotted line. This can lead to a change in intersection topography.

investigation to large systems microsolvated with up to 150 water molecules. With the QM/MM methodology, it is certainly possible to treat much larger environments; in the calculations presented here, the bottleneck is invariably the quantum mechanical region. We have investigated the accuracy of the QM/MM approximation in reproducing fully QM results for quantities of interest in the photochemical context. The conclusion is that this agreement is quite satisfactory, although this is expected to depend somewhat on the particular QM/MM decomposition chosen and should be tested in most cases. Future improvements may include the incorporation of mutual polarization of the MM and QM regions,[26,29−31,73−75] which could further improve the accuracy of the QM/MM approximations.

The biologically relevant chromophores which we have chosen in this study all involve cis−trans isomerization as one of the possible photochemical reaction channels. Therefore, as we have shown in previous work, the intersections of interest are expected to arise from the interaction of electronic states related by charge transfer.[8,9,49,68,69,76] Consequently, the primary static effect of polar solvation in these molecules is to preferentially stabilize one of these states, often resulting in cases where the conical intersection becomes an absolute minimum on the excited state potential energy surface. This behavior accentuates the funnel-like character of the intersection and is expected to lead to faster excited state decay in solution. This can be expected to be a general effect in intersections arising from electronic states related by charge transfer and is unlikely to be restricted to photoisomerization, as shown schematically in Figure 8. However, it is not a universal effect for all conical intersections; for example, at the solvated O−H stretch MECI in the GFP chromophore, both S_0 and S_1 are charge transfer states of $GFP^- - H_3O^+$ type. Thus, both are stabilized by polar solvation to approximately the same extent and the topography of the intersection does not change significantly.

As we have pointed out earlier in our applications of the semiempirical FOMO−CI method to isolated chromophores, one should be cautious in applying the method with standard parametrizations which are not designed for excited state potential energy surfaces. Nevertheless, our previous investigations showed that many of the qualitative aspects of intersection geometries and topographies are well-predicted using standard parametrizations. Thus, we expect that our conclusions about the static polar solvation effects on the photochemical energy landscape in these molecules are generally valid. Ultimately, the method is expected to be most promising in the context of reparametrization for specific molecules. It can then be applied to nonadiabatic dynamics in solution environments, and such applications to solution photochemistry are currently in progress.

Acknowledgment. Financial support for this work was provided by the National Science Foundation (CHE-02-311876 and DMR-99-76550). T.J.M. is the grateful recipient of CAREER, Beckman Young Investigator, Packard Fellow and Dreyfus Teacher-Scholar awards from NSF, Beckman, Packard and Dreyfus Foundations, respectively. VMD[77] was used to generate some of the figures.

Supporting Information Available: Coordinates for all structures described in the text with at most two water molecules (28 tables/33 pages). Nonadiabatic coupling and energy difference gradient vectors for MECIs reported in the text. This material is available free of charge via the Internet at http://pubs.acs.org. Coordinates for structures with more than two water molecules and corresponding nonadiabatic coupling and energy difference gradient vectors (78 pages) are available on request from the authors or via the Internet at http://spawn.scs.uiuc.edu/reprints/ConicQMMMSuppInfoByRequest.txt.

References and Notes

(1) Klessinger, M.; Michl, J. *Excited States and Photochemistry of Organic Molecules*; VCH Publishers: New York, 1995.
(2) Yarkony, D. R. *J. Phys. Chem. A* **2001**, *105*, 6277.
(3) Robb, M. A.; Bernardi, F.; Olivucci, M. *Pure Appl. Chem.* **1995**, *67*, 783.
(4) Celani, P.; Ottani, S.; Olivucci, M.; Bernardi, F.; Robb, M. A. *J. Am. Chem. Soc.* **1994**, *116*, 10141.
(5) Manaa, M. R.; Yarkony, D. R. *J. Am. Chem. Soc.* **1994**, *116*, 11444.
(6) Vreven, T.; Bernardi, F.; Garavelli, M.; Olivucci, M.; Robb, M. A.; Schlegel, H. B. *J. Am. Chem. Soc.* **1997**, *119*, 12687.
(7) Smith, B. R.; Bearpark, M. J.; Robb, M. A.; Bernardi, F.; Olivucci, M. *Chem. Phys. Lett.* **1995**, *242*, 27.
(8) Ben-Nun, M.; Martínez, T. J. *Chem. Phys. Lett.* **1998**, *298*, 57.
(9) Ben-Nun, M.; Quenneville, J.; Martinez, T. J. *J. Phys. Chem. A* **2000**, *104*, 5161.
(10) Quenneville, J.; Ben-Nun, M.; Martínez, T. J. *J. Photochem. Photobiol.* **2001**, *144A*, 229.
(11) Martínez, T. J. *Chem. Phys. Lett.* **1997**, *272*, 139.
(12) Marx, D.; Doltsinis, N. L. *Phys. Rev. Lett.* **2002**, *88*, 166402.
(13) Warshel, A.; Levitt, M. *J. Mol. Biol.* **1976**, *103*, 227.
(14) Gao, J. L. *Acc. Chem. Res.* **1996**, *29*, 298.
(15) Field, M. J.; Bash, P. A.; Karplus, M. *J. Comput. Chem.* **1990**, *11*, 700.
(16) Kairys, V.; Jensen, J. H. *J. Phys. Chem.* **2000**, *104*, 6656.
(17) Philipp, D. M.; Friesner, R. A. *J. Comput. Chem.* **1999**, *20*, 1468.
(18) Bryce, R. A.; Buesnel, R.; Hillier, I. H.; Burton, N. A. *Chem. Phys. Lett.* **1997**, *279*, 367.
(19) Stanton, R. V.; Little, L. R.; Merz, K. M. *J. Phys. Chem.* **1995**, *99*, 17344.
(20) Singh, U. C.; Kollman, P. A. *J. Comput. Chem.* **1986**, *7*, 718.
(21) Rothlisberger, U.; Carloni, P.; Doclo, K.; Parrinello, M. *J. Biol. Inorg. Chem.* **2000**, *5*, 236.
(22) Hayashi, S.; Ohmine, I. *J. Phys. Chem. B* **2000**, *104*, 10678.
(23) Cui, Q.; Elstner, M.; Kaxiras, E.; Frauenheim, T.; Karplus, M. *J. Phys. Chem. B* **2001**, *105*, 569.
(24) Kerdcharoen, T.; Morokuma, K. *Chem. Phys. Lett.* **2002**, *355*, 257.
(25) Vreven, T.; Menucci, B.; da Silva, C. O.; Morokuma, K.; Tomasi, J. *J. Chem. Phys.* **2001**, *115*, 62.
(26) Thompson, M. A.; Schenter, G. K. *J. Phys. Chem.* **1995**, *99*, 6374.
(27) Thompson, M. A. *J. Phys. Chem.* **1996**, *100*, 14492.

(28) Lobaugh, J.; Rossky, P. J. *J. Phys. Chem. A* **2000**, *104*, 899.
(29) Gao, J. L.; Byun, K. *Theor. Chem. Acc.* **1997**, *96*, 151.
(30) Luzhkov, V.; Warshel, A. *J. Am. Chem. Soc.* **1991**, *113*, 4491.
(31) Dupuis, M.; Aida, M.; Kawashima, Y.; Hirao, K. *J. Chem. Phys.* **2002**, *117*, 1242.
(32) Dupuis, M.; Kawashima, Y.; Hirao, K. *J. Chem. Phys.* **2002**, *117*, 1256.
(33) Kongsted, J.; Osted, A.; Mikkelsen, K. V.; Christiansen, O. *Mol. Phys.* **2002**, *100*, 1813.
(34) Kawashima, Y.; Dupuis, M.; Hirao, K. *J. Chem. Phys.* **2002**, *117*, 248.
(35) Poulsen, T. D.; Kongsted, J.; Osted, A.; Ogilby, P. R.; Mikkelsen, K. V. *J. Chem. Phys.* **2001**, *115*, 2393.
(36) Hayashi, S.; Tajkorshid, E.; Pebay-Peyroula, E.; Royant, A.; Landau, E. M.; Navarro, J.; Schulten, K. *J. Phys. Chem. B* **2001**, *105*, 10124.
(37) Rajamani, R.; Gao, J. *J. Comput. Chem.* **2002**, *23*.
(38) Vreven, T.; Morokuma, K. *J. Chem. Phys.* **2000**, *113*, 2969.
(39) Grabo, T.; Petersilka, M.; Gross, E. K. U. *J. Mol. Struct (THEOCHEM)* **2000**, *501*, 353.
(40) Docken, K. K.; Hinze, J. *J. Chem. Phys.* **1972**, *57*, 4928.
(41) Roos, B. O. The Complete Active Space Self-Consistent Field Method and its Applications in Electronic Structure Calculations. In *Advances in Chemical Physics: Ab Initio Methods in Quantum Chemistry II*; Lawley, K. P., Ed.; John Wiley and Sons Ltd.: New York, 1987; p 399.
(42) Garavelli, M.; Frabboni, B.; Fato, M.; Celani, P.; Bernardi, F.; Robb, M. A.; Olivucci, M. *J. Am. Chem. Soc.* **1999**, *121*, 1537.
(43) Ben-Nun, M.; Martínez, T. J. *J. Chem. Phys.* **1998**, *108*, 7244.
(44) Granucci, G.; Persico, M.; Toniolo, A. *J. Chem. Phys.* **2001**, *114*, 10608.
(45) Tully, J. C. *J. Chem. Phys.* **1990**, *93*, 1061.
(46) Granucci, G.; Toniolo, A. *Chem. Phys. Lett.* **2000**, *325*, 79.
(47) Hunt, W. J.; Goddard, W. A., III. *Chem. Phys. Lett.* **1969**, *3*, 414.
(48) Bone, R. G. A.; Pulay, P. *Int. J. Quantum Chem.* **1993**, *45*, 133.
(49) Toniolo, A.; Ben-Nun, M.; Martinez, T. J. *J. Phys. Chem. A* **2002**, *106*, 4679.
(50) Persico, M.; Granucci, G.; Inglese, S.; Laino, T.; Toniolo, A. *J. Mol. Struct. (THEOCHEM)* **2003**, *621*, 119.
(51) Dewar, M. J. S.; Liotard, D. A. *J. Mol. Struct (THEOCHEM)* **1990**, *65*, 123.
(52) Segal, G. A. *Semiempirical methods of electronic structure calculation*; Plenum Press: New York, 1977.
(53) Hinchliffe, A. *Modelling molecular structures*; J. Wiley: Chichester, 1994.
(54) Stewart, J. J. P. MOPAC2000; Fujitsu Limited: Tokyo, Japan, 1999.
(55) Bearpark, M. J.; Robb, M. A.; Schlegel, H. B. *Chem. Phys. Lett.* **1994**, *223*, 269.
(56) Dewar, M. J. S.; Zoebisch, E. G.; Healy, E. F.; Stewart, J. J. P. *J. Am. Chem. Soc.* **1985**, *107*, 3902.
(57) Weiner, S. J.; Kollmann, P. A.; Case, D. A.; Singh, U. C.; Ghio, C.; Alagona, G.; Profeta, S.; Weiner, P. *J. Am. Chem. Soc.* **1984**, *106*, 765.
(58) Dang, L. X.; Pettitt, B. M. *J. Phys. Chem.* **1987**, *91*, 3349.
(59) Antes, I.; Thiel, W. *J. Phys. Chem. A* **1999**, *103*, 9290.
(60) Zimmer, M. *Chem. Rev.* **2002**, *102*, 759.
(61) Weber, W.; Helms, V.; McCammon, J. A.; Langhoff, P. W. *Proc. Natl. Acad. Sci.* **1999**, *96*, 6177.
(62) Olsen, S.; Manohar, L.; Martinez, T. J. Work in progress.
(63) Litvinenko, K. L.; Webber, N. M.; Meech, S. R. *Chem. Phys. Lett.* **2001**, *346*, 47.
(64) Pellequer, J.-L.; Wager-Smith, K. A.; Kay, S. A.; Getzoff, E. D. *Proc. Natl. Acad. Sci.* **1998**, *95*, 5884.
(65) Ryan, W. L.; Gordon, D. J.; Levy, D. H. *J. Am. Chem. Soc.* **2002**, *124*, 6194.
(66) Hoff, W. D.; Devreese, B.; Fokkens, R.; Nugteren-Roodzant, I.; Van Beeumen, J. J.; Nibbering, N.; Hellingwerf, K. J. *Biochemistry* **1996**, *35*, 1274.
(67) Baca, M.; Borgstahl, G. E. O.; Boissinot, M.; Burke, P. M.; Williams, D. R.; Slater, K. A.; Getzoff, E. D. *Biochemistry* **1994**, *33*, 14369.
(68) Ben-Nun, M.; Martínez, T. J. *Chem. Phys.* **2000**, *259*, 237.
(69) Ben-Nun, M.; Molnar, F.; Schulten, K.; Martinez, T. J. *Proc. Natl. Acad. Sci.* **2002**, *99*, 1769.
(70) Atchity, G. J.; Xantheas, S. S.; Ruedenberg, K. *J. Chem. Phys.* **1991**, *95*, 1862.
(71) Yarkony, D. R. *J. Chem. Phys.* **2001**, *114*, 2601.
(72) Matsika, S.; Yarkony, D. R. *J. Chem. Phys.* **2001**, *115*, 5066.
(73) Thompson, M. A. *J. Am. Chem. Soc.* **1995**, *117*, 11341.
(74) Hillier, I. H. *J. Mol. Struct (THEOCHEM)* **1999**, *463*, 45.
(75) Stern, H. A.; Kaminski, G. A.; Banks, J. L.; Zhou, R.; Berne, B. J.; Friesner, R. A. *J. Phys. Chem. B* **1999**, *103*, 4730.
(76) Molnar, F.; Ben-Nun, M.; Martínez, T. J.; Schulten, K. *J. Mol. Struct (THEOCHEM)* **2000**, *506*, 169.
(77) Humphrey, W.; Dalke, A.; Schulten, K. *J. Mol. Graph.* **1996**, *14*, 33.